This is a pre print version of the following article:

Effectiveness investigation of HPFRCC strengthening layers through a time-dependent mechanical model / Sanchez, J., Savino, V., Lanzoni, L., Tarantino, A.M., Viviani, M.. - In: COMPOSITE STRUCTURES. - ISSN 0263-8223. - 121119:(2026), pp. 1-14. [10.1016/j.compstruct.2026.121119]

Terms of use:

The terms and conditions for the reuse of this version of the manuscript are specified in the publishing policy. For all terms of use and more information see the publisher's website.

24/11/2026 07:37

(Article begins on next page)

Composite Structures xxx (xxxx) 121119

Contents lists available at ScienceDirect

Composite Structures

journal homepage: www.elsevier.com/locate/compstruct

Effectiveness investigation of HPFRCC strengthening layers through a time-dependent mechanical model

J.A.L. Sanchez [a], V. Savino [a], L. Lanzoni [b,*], A.M. Tarantino [b], M. Viviani [a]

[a] School of Engineering and Management Vaud, HES-SO University of Applied Sciences and Arts Western Switzerland, Route de Cheseaux 1, CH-1401 Yverdon-Les-Bains, Switzerland

[b] Department of Engineering "Enzo Ferrari", University of Modena and Reggio Emilia, 41125 Modena, Italy

ARTICLE INFO

Keywords:
Bonding mechanism
Contact problem
Composite layers
Interface stress
Cohesive modelling
Creep modeling

ABSTRACT

High-performance fiber-reinforced cementitious composites (HPFRCCs) are increasingly used as strengthening overlays for reinforced concrete (RC) structures. While their short-term behavior is well documented, the long-term response of the interface between existing concrete and HPFRCC overlays remains a challenging issue. This paper proposes a time-dependent mechanical model to predict the evolution of stresses, strains, and slip at the interface of RC members strengthened with HPFRCC layers. The model combines a linear viscoelastic formulation accounting for creep and shrinkage of both materials with an experimentally calibrated cohesive law governing the interfacial bond response. An experimental campaign on a small-scale normal-strength concrete (NSC)–HPFRCC composite beam subjected to sustained loading is conducted to validate the model, showing good agreement between measured and predicted slip evolution over six months. Numerical results highlight that differential creep and shrinkage induce significant stress redistribution over time, with tensile stresses in the NSC increasing by more than 2000% from a very low initial level while remaining below the material tensile strength under the investigated service conditions. A sensitivity analysis further shows that very small interface slip is consistent with a highly stiff connection but should not be interpreted independently from interface stiffness, strength and deformation capacity.

1. Introduction

The rehabilitation and strengthening of existing reinforced concrete (RC) infrastructures has become a critical challenge worldwide due to ageing assets, increasing service demands, and sustainability constraints. Among the available techniques, the application of thin strengthening overlays based on high-performance fiber-reinforced cementitious composites (HPFRCCs) has gained increasing attention. HPFRCC overlays offer high mechanical performance, enhanced durability, and limited additional dead load, making them particularly attractive for bridge decks, slabs, and beams exposed to aggressive environments [1–7]. Moreover, extending the service life of infrastructure while reducing its susceptibility to degradation and maintenance demand represents a key contribution to sustainable construction practice [8–11].

Despite extensive research demonstrating the short-term structural benefits of HPFRCC strengthening systems, premature deterioration and debonding at the interface between the existing concrete substrate and the strengthening layer are still reported in practice. Experimental observations and field evidence indicate that interfacial distress may develop even when external loads remain within serviceability limits. These phenomena are primarily associated with differential shrinkage and creep between the substrate and the overlay, combined with sustained loading during service life [12,13].

Most existing numerical and analytical studies on HPFRCC- or UHPC-strengthened RC members either assume a perfect bond at the interface or focus on short-term mechanical response [4,14]. While such assumptions may be acceptable for ultimate limit state analyses, they can significantly underestimate long-term interfacial stresses and overestimate durability. More refined approaches have introduced cohesive or fracture-based interface models, enabling a more realistic representation of bond behavior under mixed-mode loading conditions [15–18]. However, these models are typically calibrated at early age and neglect the time-dependent evolution of material properties and interfacial demand.

Time-dependent effects at material interfaces have been investigated in other composite systems, such as FRP–concrete joints or steel–concrete composite beams, where viscoelastic formulations have been suc-

* Corresponding author at: DIEF-Department of Engineering "Enzo Ferrari", University of Modena and Reggio Emilia, 41125 Modena, Italy.
E-mail address: luca.lanzoni@unimo.it (L. Lanzoni).

https://doi.org/10.1016/j.compstruct.2026.121119
Received 5 May 2026; Received in revised form 26 August 2026; Accepted 12 November 2026
0263-8223/© 20XX

UNCORRECTED PROOF

cessfully employed to capture stress redistribution over time [19–23]. Nevertheless, the direct transfer of these approaches to cement-based strengthening systems is not straightforward, due to the pronounced creep and shrinkage of both bonded materials and the mixed-mode nature of interfacial stresses in concrete overlays. To date, a generalized mechanical framework capable of describing the long-term interfacial response of HPFRCC-strengthened RC members, grounded on experimentally measured bond laws, remains lacking.

This paper addresses this gap by proposing a time-dependent mechanical model for RC members strengthened with HPFRCC layers under sustained loading. The model combines a linear viscoelastic formulation accounting for creep and shrinkage of both the existing concrete substrate and the HPFRCC overlay with an experimentally calibrated cohesive law governing interfacial shear behavior [18,23]. The approach enables the prediction of stress migration, slip evolution, and strain redistribution at the interface over the service life of composite members.

Particular attention is devoted to the mechanical significance of the very small relative displacements developing at highly stiff cementitious interfaces. In addition to experimental validation, a sensitivity analysis is therefore performed to investigate how interface stiffness governs the interaction among relative sliding, internal force transfer and stress redistribution. This allows interface slip to be interpreted in relation to stiffness, strength and deformation capacity, rather than as an independent indicator of interface performance.

An experimental campaign on a small-scale normal-strength concrete (NSC)–HPFRCC composite beam, specifically designed for laboratory testing while remaining representative of relevant structural applications, was carried out to validate the proposed model. This specimen was strengthened with a HPFRCC overlay and then subjected to long-term loading. Measured slip evolution over six months is compared with numerical predictions, demonstrating good agreement. The validated model is then employed to investigate the long-term evolution of interfacial stresses and to assess the risk of delayed debonding under service-level loads.

The proposed framework provides a physically based general tool for evaluating the durability of HPFRCC-strengthened RC members, with direct implications for the design of strengthening layers, the assessment of bond reliability, and the planning of inspection and maintenance strategies.

2. Materials and methods

To investigate the time-dependent stress evolution in retrofitted composite concrete members, an experimental program representative of field applications was designed. A concrete specimen representative of an existing substrate was first cast and cured. After curing, the top surface was prepared by hydro-jetting, a technique commonly adopted in the rehabilitation of concrete structures to enhance interfacial bond performance [18]. A commercial HPFRCC was then cast as a thin strengthening overlay onto the prepared substrate surface, forming a composite element representative of strengthened members. After casting, the specimens were cured for 28 days under controlled environmental conditions prior to testing, ensuring stable mechanical properties of the strengthening layer.

2.1. Preparation of samples

The existing substrate of the composite members was simulated by manufacturing a plain normal-strength concrete (NSC), representative of concrete commonly employed in slabs on grade, bridge decks and pavements (Fig. 1). The mix design complied with SN EN 206 and was prepared using a vertical-shaft Zyklos mixer. A $500 \times 100 \times 1100\ mm^3$ NSC slab was cast, together with six $150 \times 150 \times 150\ mm^3$ cubic specimens realized for compressive strength determination. Knowledge of the substrate compressive strength was required to select the appropriate hydro-jetting pressure for surface preparation [18].

After casting, the fresh concrete was vibrated to ensure homogeneity and then cured under controlled environmental conditions (20 ± 2 °C, $55 \pm 5\%$ RH). The fresh and hardened material properties of the NSC substrate, together with those of the HPFRCC overlay, are reported in Table 1 [18]. After 28 days, the slab was demolded and cut into five $100 \times 100 \times 1100\ mm^3$ prismatic beams, which were subsequently stored in a climatic chamber to simulate an additional natural ageing of six months.

Prior to application of the strengthening layer, the top surface of the NSC beams was treated by hydro-jetting. The resulting roughness profile, characterized by peak-to-valley amplitudes of approximately 1–2 cm, is shown in Fig. 2 and it was verified by photogrammetric analysis [18]. Following surface preparation, the substrate was cleaned and conditioned to a saturated-surface-dry (SSD) state. Previous studies have shown that SSD conditions promote optimal short-term bond strength



Fig. 1. Pouring of NSC substrate to make $500 \times 100 \times 1100$ mm slab.

Table 1
Fresh and hardened material properties of NSC substrate and HPFRCC overlay.

Properties	Substrate (NSC)	Overlay (HPFRCC)
Maximum aggregate size (mm)	16	6
Water/cement ratio	0.4	0.28
Slump test (mm)	700	240
Slump test T500 (mm)	–	60
Compressive strength (MPa)	38.4 ± 0.3	80.4 ± 4
Tensile strength (MPa)	2.9[a]	6 ± 1.8
Young's modulus (MPa)	32950[a]	33800 ± 700

[a] Calculated using the European standard formula [24].

for HPFRCC overlays [18,25]. SSD was achieved by conditioning the substrate surface under controlled conditions for 14 days, during which carbonation was limited by covering the surface with a plastic film [26]. Surface moisture was monitored using an embedded relative humidity probe.

A commercial high-performance fiber-reinforced cementitious composite (HPFRCC) was used as strengthening overlay. Mixing and casting procedures followed the manufacturer's specifications and relevant European standard [27] as well. After placement, the overlay was compacted to minimize entrapped air, particularly in the interfacial transition zone, which strongly influences bond development. From the same batch, cubic ($150 \times 150 \times 150\ mm^3$), prismatic ($40 \times 40 \times 160\ mm^3$) and dog-bone specimens were cast to characterize the mechanical properties of the HPFRCC. The mix design and engineering properties of the HPFRCC are listed in Table 1 and Table 2.

After 28 days of curing under controlled conditions, the composite NSC–HPFRCC beams were subjected to instantaneous and long-term loading tests. The geometry and main characteristics of the composite beams are listed in Table 3. The experimentally measured material and interfacial parameters were subsequently implemented in the time-dependent cohesive model described in Section 2.3. Creep functions and shrinkage laws adopted to describe the long-term behaviour of NSC and HPFRCC are taken from [29].

2.2. Test setup

2.2.1. Mechanical properties of single bonded materials

The mechanical properties of each material composing the composite system were experimentally characterized prior to testing the strengthened members. The compressive strength of cubic NSC and HPFRCC specimens was measured using a force-controlled computerized testing machine at a loading rate of 0.6 MPa/s, in accordance with the relevant European standard [30].

Table 2
Compounds in NSC substrate and HPFRCC overlay.

Compounds	Substrate (NSC) kg/m^3	Overlay (HPFRCC)
Premix[a] (cement, silica fume, sand)	–	2135
Portland cement	315	–
Fine aggregate 0–4 mm	803.6	–
Fine aggregate 4–8 mm	150.6	–
Coarse aggregate 8–16 mm	378.3	–
Coarse aggregate 16–32 mm	568	–
Water	183.7	230
Superplasticizer[a]	–	21.3
Hooked steel fibers[a] 30/0.6 mm	–	25 (0.3%)

[a] Further details on the HPFRCC are reported in [28].

Direct tensile strength and Young's modulus of the HPFRCC were determined using a displacement-controlled testing device on dog-bone and prismatic specimens, respectively, following European standards [31,32]. Dog-bone specimens were subjected to an axial displacement rate of 0.05 ± 0.01 mm/min. Axial strains were measured using a high-precision strain gauge bonded to the specimen surface, with a data acquisition frequency of 10 Hz [33]. The experimental setups adopted for the different material tests are shown in Fig. 3.

2.2.2. Mechanical behaviour of composite members and definition of service load

In order to investigate the time-dependent stress evolution of NSC–HPFRCC composite beams under service conditions, it was first necessary to characterize their short-term mechanical response up to failure. This preliminary phase allowed the definition of a load level representative of service conditions and provided experimental data required for calibrating the parameters implemented in the mechanical model described in Section 2.3.

Three composite NSC–HPFRCC beams with dimensions $100 \times 100 \times 550\ mm^3$ were tested under monotonically increasing load using a three-point bending configuration (3PBFT), in accordance with European standard provisions [27]. The tests were performed using a displacement-controlled testing machine. The applied load was recorded through a calibrated hydraulic load cell, while the mid-span deflection and the crack mouth opening displacement (CMOD) at the bottom fiber were continuously monitored using a digital acquisition system. The CMOD was controlled to increase at a rate of 0.05 ± 0.01 mm/min, and both load and CMOD were sampled at 10 Hz



Fig. 2. Surface of the substrate NSC beams after hydro-jetting.

CORRECTED PROOF

Table 3
Geometrical properties of experimental composite beam.

Length of the beam (mm)	1100
Height of HPFRCC layer (mm)	30
Height of NSC layer (mm)	70
NSC area (mm^2)	7'000
HPFRCC area (mm^2)	3'000
Moment of inertia of the NSC layer (mm^4)	2.858×10^6
Moment of inertia of the HPFRCC layer (mm^4)	225'000
Concentrated load (kN)	0.25
Initial and final time for viscoelastic analysis	t_0 = 28 days, t_∞ = 25'550 days (i.e. 70 years)
Creep function and shrinkage laws to describe the long-term behaviour of NSC and HPFRCC	[29]
Environmental conditions used for the experiments	T = 20 ± 2 °C, RH = 55 ± 5%

throughout the test. The HPFRCC layer was positioned on the tension side of the beam, as premature debonding in practice predominantly occurs when the strengthening overlay is subjected to tensile stresses [22]. The load–CMOD responses obtained from the 3PBFT are reported in Fig. 4. An elastic response was consistently observed for CMOD values lower than 0.1 mm, which is representative of service conditions in composite members. Within this range, the global structural response of the beam can be considered linear.

However, a globally linear response does not necessarily imply that the interfacial shear stresses remain within the linear elastic range of the bond law. To verify the validity of applying linear viscoelasticity at the interface, the shear stress acting in mode II along the NSC–HPFRCC interface was analytically estimated using the formulation presented in Section 2.3. The computed interfacial shear stresses were then compared with the experimentally determined shear stress–slip constitutive law obtained from direct shear bond tests on NSC–HPFRCC interfaces [18], as shown in Fig. 5. In those tests, pure mode II loading was ensured by using non-fixed loading and supporting rollers, which were free to translate and thus automatically aligned with the applied force. This configuration minimized load eccentricity and the associated bending moments and normal stresses at the interface [18], allowing the measured response to reflect predominantly shear transfer.

The experimentally determined bond law exhibits an initial approximately linear elastic branch up to a slip of about 0.005 mm, followed by a nonlinear softening response. The initial branch corresponds to a secant shear stiffness K_{II} of approximately 1354 MPa/mm. The combination of high interface stiffness and limited displacement capacity implies that significant shear stresses can be mobilised for relative displacements of only a few micrometres. Consequently, micrometric slip values should not necessarily be regarded as mechanically negligible or, by themselves, as an indication of low interfacial demand.

The interface constitutive parameters were calibrated directly from

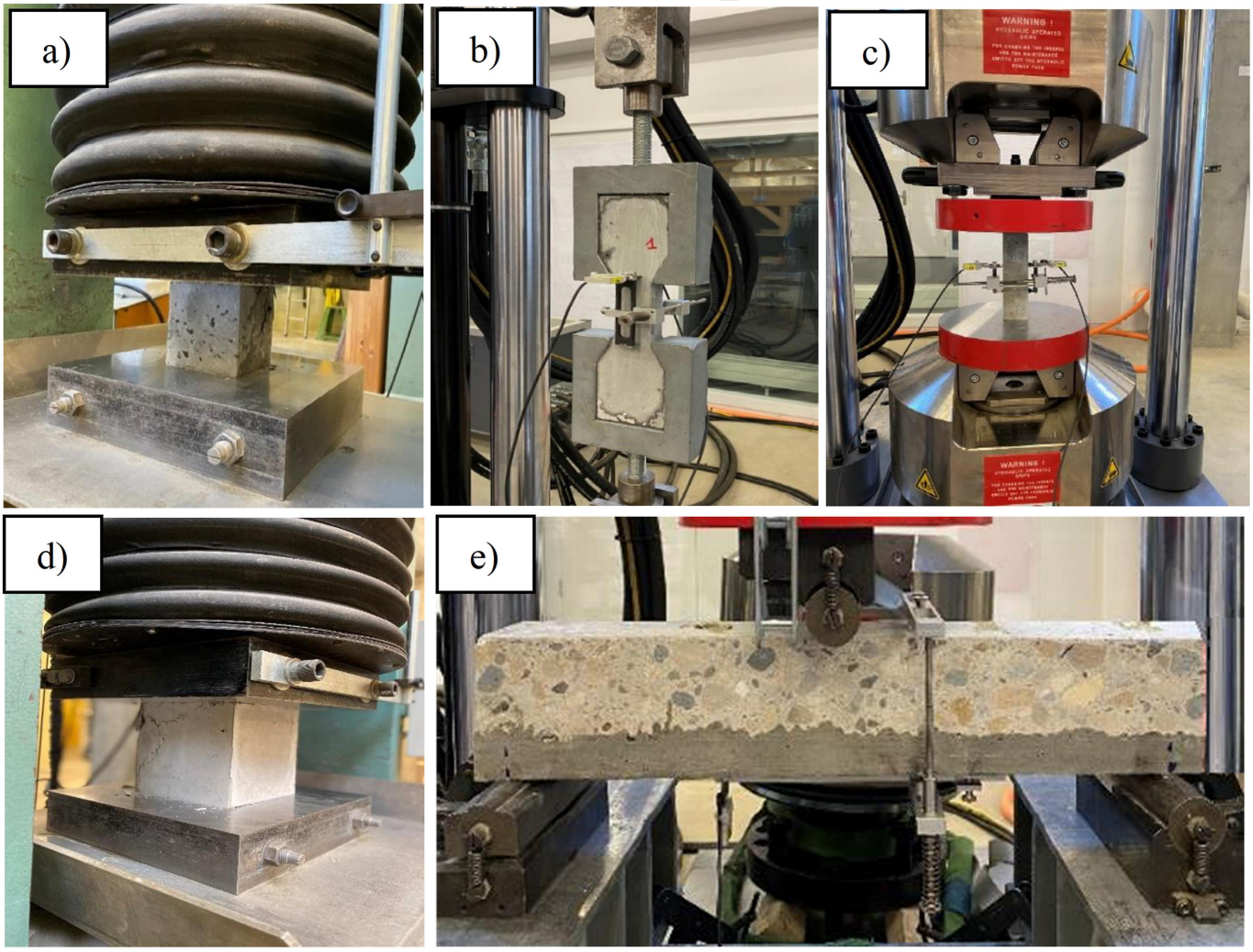

Fig. 3. Photos showing the set-up of experimental tests carried out at HEIG-VD laboratory for measuring: a) compressive strength of HPFRCC cubes, b) direct tensile strength of HPFRCC dog-bones, c) Young's modulus of HPFRCC prisms, d) compressive strength of NSC cubes, e) scale 100 × 100 × 550 mm3 NSC-HPFRCC composite beams subjected to 3PBF loads.

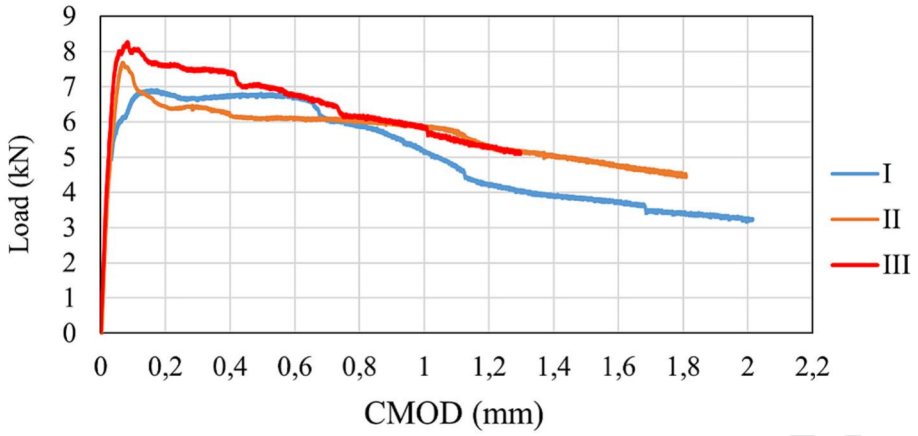

Fig. 4. Load-Cracking mouth open displacement (CMOD) diagram obtained by testing 3 composite NSC-HPFRC beams under 3PBF loads in agreement with European standard [27].

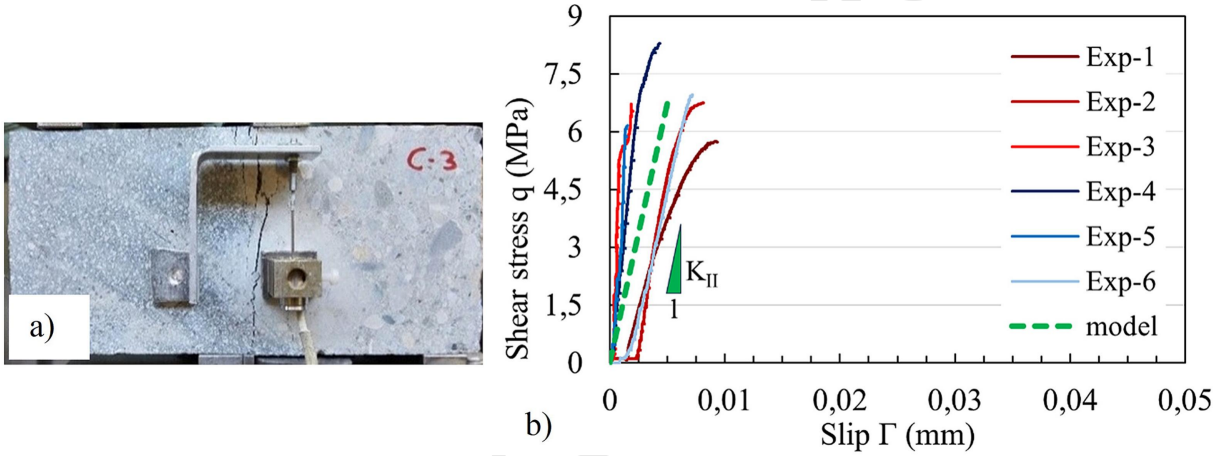

Fig. 5. Stress-slip pattern governing the mode II along the NSC-HPFRCC interface: (a) Failure mode during the direct shear bond test on scale samples, (b) Experimental results in terms of shear stress q [MPa] (mode II) vs slip Γ [mm] along the interface [18].

the experimental results reported in [18,34], where the NSC–HPFRCC interface was characterised through multiple shear/bond tests combined with photogrammetric analysis of the surface morphology. The pronounced peak-to-valley roughness generated by hydro-jetting (approximately 1–2 cm) promotes mechanical interlock and contributes to the shear-transfer mechanism. Although the present model does not explicitly reproduce the three-dimensional roughness geometry, its influence is implicitly incorporated through the experimentally calibrated interface constitutive parameters, particularly the initial shear stiffness and peak shear strength. In order to ensure that the interface behaviour remains within the linear elastic range, an iterative load calibration procedure was adopted. Starting from a load level within the elastic portion of the 3PBFT response, the corresponding interfacial shear stress was computed and compared with the elastic peak of the bond law. The applied load was progressively reduced until the computed shear stress was lower than 40% of the peak shear stress, in agreement with recommendations reported in [35].

The configuration shown in (Fig. 6) represents the negative-moment region above an internal support, where the strengthening overlay is located on the upper tensile side of the member. Rather than reproducing a complete multi-span system, the portion between the adjacent zero-moment sections was idealised as a simply supported specimen and inverted for laboratory testing. It is remarked that the bending test was not intended as statistical replicates of a single loading condition, but as complementary mechanics-oriented experiment aimed at investigating the time-dependent NSC–HPFRCC interface response under representative bending conditions of continuous structural members. Accordingly, the experimental program provides a mechanic-based assessment of the long-term interface response rather than a statistically exhaustive structural-scale validation.

The composite beam was instrumented with 11 displacement gauges (precision of ± 2 μm) positioned along the beam length on both sides, as close as possible to the interface. This arrangement was necessary due to the pronounced roughness of the hydro-jetted interface. Additionally, a vertical displacement gauge was installed at the beam extrados to measure the mid-span deflection (precision of ±2 μm).The specimen was stored under controlled laboratory conditions (20 ± 2 °C, 55 ± 5% RH), and the evolution of interfacial slip was monitored over a period of six months, in accordance with standard recommendations [35]. The environmental conditions were intentionally kept constant throughout the monitoring period in order to isolate the mechanical effects of sustained loading and differential creep between the substrate and the strengthening layer. Although real structures are exposed to variable climatic conditions, the adoption of controlled laboratory conditions is consistent with standard creep testing procedures and provides a reproducible basis for validating the proposed mechanical model.

2.3. Time-dependent cohesive model

The long-term behaviour of the NSC–HPFRCC composite beam is simulated by adopting creep and shrinkage formulations for both materials in accordance with the European standard [29], which is appropriate

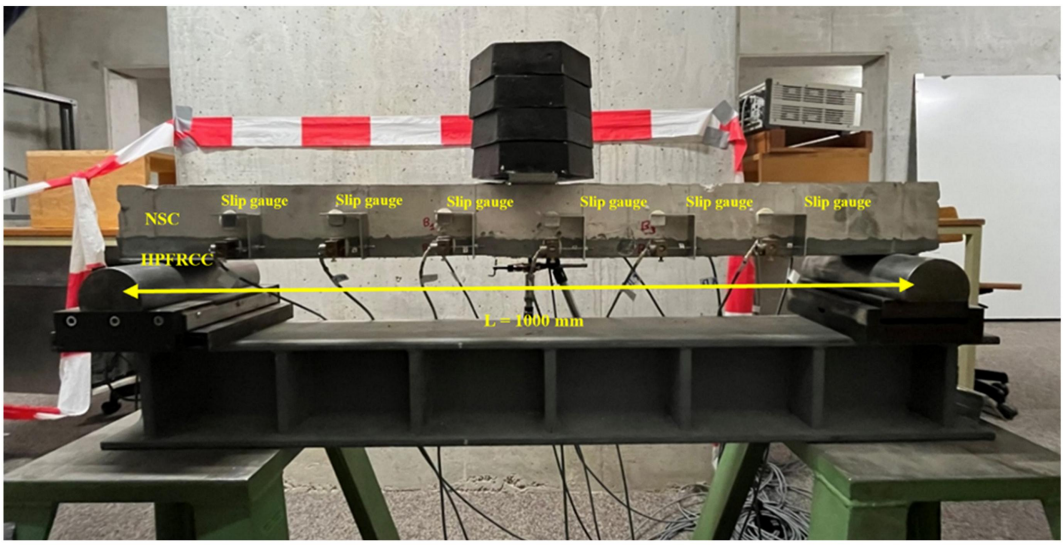

a)

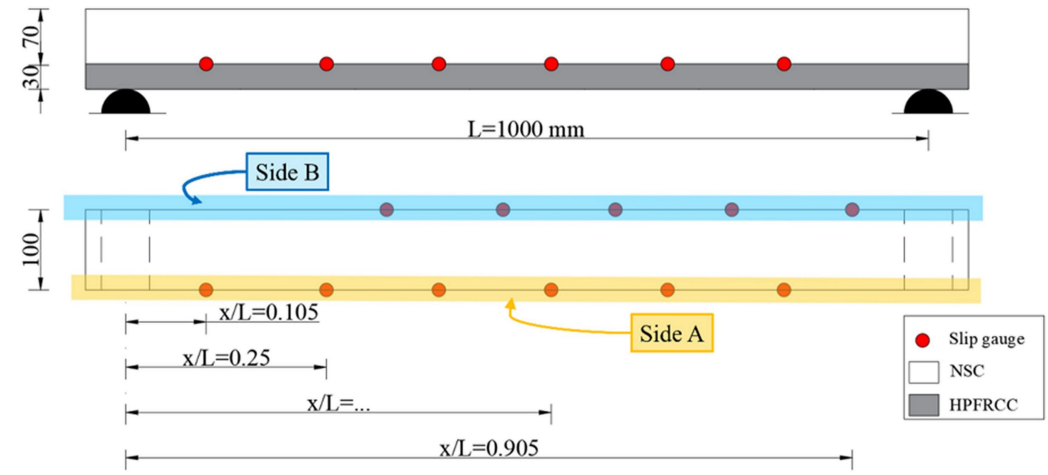

b)

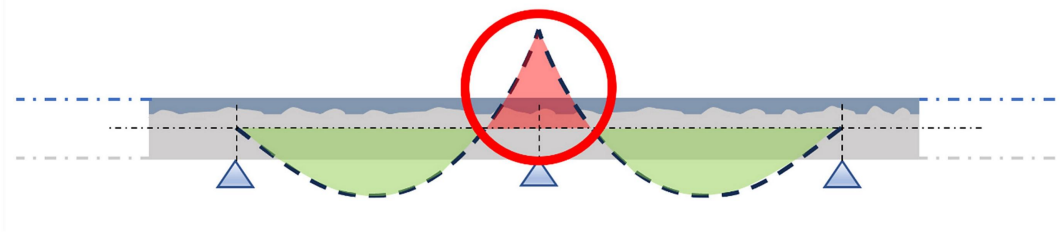

c)

Fig. 6. a) Setup of LT-3PBFT (side A) carried out at HEIG-VD laboratory (Switzerland). A small-scale 1100 × 100 × 100 mm composite beam is equipped by strain gauges for recording the slip evolution along the interface, b) Schematization of the acquisition system with quotes in mm, c) Schematic representation of a multi-span beam, representative of a continuous deck or slab strengthened with a top overlay: negative-moment region over an internal support (red) and positive-moment region between adjacent supports (green).

for service–level stress conditions. The strain–stress analysis of the composite system is based on a coupled mechanical formulation combining equilibrium conditions, compatibility relations, and constitutive laws for the substrate, the strengthening layer, and the interface.

The governing system of equations consists of:

(i) equilibrium equations (Eq. (1)),
(ii) compatibility equations (Eq. (2)), and
(iii) constitutive relationships for the interface and the bonded materials (Eqs. 3–5). The present formulation does not account for nonlinear constitutive effects at the interface, such as softening or damage evolution, and relies on a linearized shear stress–slip relationship consistent with the service-level conditions considered. Once the corresponding failure criterion is reached, the nonlinear evolution of the interface requires cohesive damage laws capable of representing crack initiation, mixed-mode interaction and

subsequent propagation. Such a formulation has already been developed by the Authors in previous studies through a mixed-mode cohesive interface model capable of simulating crack initiation and propagation under combined normal and shear loading [18,34].

The solution is obtained using a numerical step-by-step procedure discretized in both space (along the beam axis) and time.

These assumptions define the pre-damage regime considered in the present formulation. In particular, the imposed transverse compatibility between the NSC and HPFRCC layers excludes local interface opening and post-debonding mechanisms. The model therefore describes the evolution of the bonded composite system up to the onset of interface damage, whereas subsequent damage initiation and propagation require the nonlinear mixed-mode cohesive formulation previously developed by the Authors.

The following assumptions are adopted in the formulation of the model:

- for both layers, plane sections rotate as rigid planes around the neutral axis (Euler–Bernoulli hypothesis);
- vertical displacements of the NSC and HPFRCC layers are identical;
- the connection between the NSC substrate and the strengthening layer is continuously distributed along the beam axis and ensured by bond development during curing;
- interfacial slip is linearly related to interfacial shear stress within the elastic range of the experimentally measured bond law;
- the beam is prismatic with constant cross-section long its length.

2.3.1. Equilibrium equations

The equilibrium of a generic cross-section of the composite beam is described by axial force and bending moment balance. As schematically sketched in Fig. 7, N_{NSC}, M_{NSC}, N_{HPFRCC}, M_{HPFRCC} denote the axial forces and bending moments in the NSC and HPFRCC layers, respectively, while N and M represent the internal actions of the composite section.

The system is modelled as a simply supported beam over a span of 1000 mm subjected to a concentrated load acting at midspan, reproducing the three-point bending experimental configuration. Owing to the symmetry of the geometry and loading, only half of the specimen is analysed. The numerical solution is obtained by imposing zero vertical displacement at the support and zero bending moment at x = 0 (M(0,t) = 0).

It is worth noting that the simply supported scheme reproduces the effects induced by the negative-moment region of a continuous deck or slab, with the supports idealising the zero-moment sections bounding the strengthened zone.

The equilibrium conditions are expressed by Eqs. (1a) and (1b):

$$N_{NSC}(x,t) = -N_{HPFRCC}(x,t) = N(x,t); \tag{1a}$$

$$M_{NSC}(x,t) + M_{HPFRCC}(x,t) + N(x,t)\,h_0 = M(x,t). \tag{1b}$$

2.3.2. Compatibility equation

Compatibility is enforced by assuming that the curvature of the NSC substrate and the HPFRCC strengthening layer is identical, owing to perfect bond between the two materials [18] along the y direction. Let E_{NSC}, I_{NSC}, E_{HPFRCC}, I_{HPFRCC} denote the Young's moduli and second moments of area of the two layers, whose values are reported in Table 3. The compatibility condition is expressed by Eq. (2):

$$\frac{M_{NSC}(x,t)}{E_{NSC}(t)\,I_{NSC}} = \frac{M_{HPFRCC}(x,t)}{E_{HPFRCC}(t)\,I_{HPFRCC}} = \frac{M(x,t) - N(x,t)\,h_0}{E_{NSC}(t)\,I_{NSC} + E_{HPFRCC}(t)\,I_{HPFRCC}}. \tag{2}$$

2.3.3. Strain and stress evaluation

Once the internal axial force and bending moments are known, the strain fields at the interface fibers of both materials can be computed. The strains ε_{NSC} and ε_{HPFRCC} correspond to the bottom fiber of the NSC layer and the top fiber of the HPFRCC layer, respectively. The geometrical parameters h_0, h_{NSC}, h_{HPFRCC} are defined in Fig. 7. The strain expressions are given by Eqs. (3a) and (3b):

$$\varepsilon_{NSC}(x,t) = -\frac{N(x,t)}{E_{NSC}(t)\,A_{NSC}} + \frac{M_{NSC}(x,t)}{E_{NSC}(t)\,I_{NSC}}\,h_{NSC} \tag{3a}$$

$$\varepsilon_{HPFRCC}(x,t) = -\frac{N(x,t)}{E_{HPFRCC}(t)\,A_{HPFRCC}} + \frac{M_{HPFRCC}(x,t)}{E_{HPFRCC}(t)\,I_{HPFRCC}}\,h_{HPFRCC} \tag{3b}$$

The corresponding stresses at the interface fibers are obtained by multiplying the strains by the time-dependent Young's moduli of the materials, as expressed by Eqs. (4a) and (4b):

$$\sigma_{NSC}(x,t) = \varepsilon_{NSC} E_{NSC}(t) \tag{4a}$$

$$\sigma_{HPFRCC}(x,t) = \varepsilon_{HPFRCC} E_{HPFRCC}(t) \tag{4b}$$

2.3.4. Interfacial slip law

Within the elastic range of the interface response, the slip Γ along the NSC–HPFRCC interface is assumed to be linearly related to the interfacial shear stress q through the shear stiffness (K_{II}) that is experimentally determined from direct shear bond tests on NSC–HPFRCC interfaces (Fig. 5), while Γ and q are computed by the model. This relationship is expressed by Eq. (5a):

$$\Gamma(x,t) = \frac{q(x,t)}{K_{II}} = \frac{\delta N(x,t)}{K_{II}\delta x}. \tag{5a}$$

The spatial derivative of the slip field is directly related to the difference between axial strains in the HPFRCC and NSC layers, as expressed by Eq. (5b). This formulation provides a direct link between the numerically computed slip and the experimentally measured slip along the interface, by introducing Eqs. (3a) and (3b) into Eq. (5b):

$$\frac{\delta\Gamma(x,t)}{\delta x} = \frac{\delta^2 N(x,t)}{K_{II}\delta x^2} = \varepsilon_{HPFRCC}(x,t) - \varepsilon_{NSC}(x,t). \tag{5b}$$

Differentiating Eq. (5b) with respect to x and introducing Eq. (5a) yields the second-order governing differential equation that directly couples the interface shear behaviour to the bulk bending and axial rigidity of the composite member.

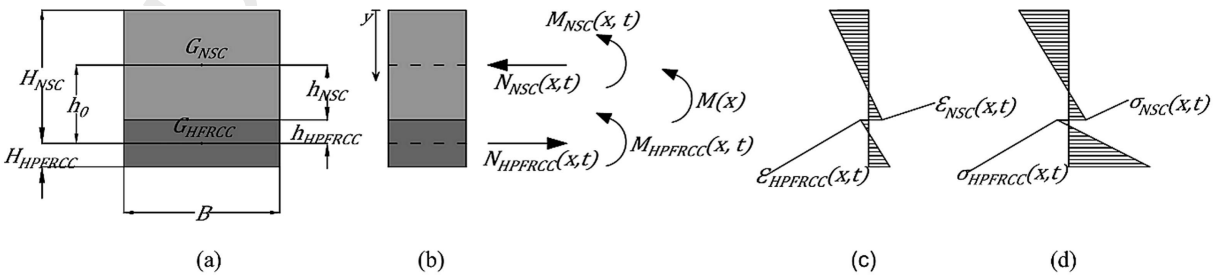

Fig. 7. Sketch of the generic cross-section of NSC-HPFRCC composite beam along the beam axis (a), decomposition of internal actions (b), strain field (c), stress field (d).

UNCORRECTED PROOF

2.3.5. Time-dependent material behaviour

The Young's modulus of both NSC and HPFRCC evolves over time due to creep. The time-dependent modulus E(t) is computed from the creep function $\phi(t,t_0)$ defined in [29], as expressed by Eq. (6):

$$\frac{1}{E(t)} = \frac{1}{E(t_0)} + \frac{\varphi(t,t_0)}{E_i}, \tag{6}$$

where $E(t_0)$ is the Young's modulus at the time of load application t_0; E_i is the Young's modulus at 28 days.

At the time of application of the external load (t_0 = 28 days after casting of the HPFRCC overlay), creep strains are assumed to be zero, and the response of both layers is elastic. This allows the governing equations to be used for short-term analysis. For $t > t_0$, creep and shrinkage effects are progressively introduced through time-dependent material properties.

2.3.6. Numerical solution and relation to previous work

In previous steel–concrete composite models, such as [23], the substrate behaves as an elastic, creep-free material and the interfacial slip law is prescribed by design codes, reflecting the mechanical anchorage of steel connectors. When extending the same framework to NSC–HPFRCC composite members, two fundamental modifications are required. First, both layers are cement-based materials and therefore exhibit time-dependent behaviour; creep and shrinkage must be defined for NSC and HPFRCC, whereas in steel-concrete systems only the concrete layer contributes to long-term deformations. This difference significantly affects the redistribution of stresses and the evolution of interfacial slip under sustained loading. Second, the bond mechanism in cement-based interfaces is governed by mechanical interlock and adhesion between two cementitious matrices, not by steel connectors. As a consequence, code-based slip laws developed for steel-concrete members [29] are not applicable. The interfacial constitutive law adopted here is therefore directly calibrated from shear bond tests performed on real NSC–HPFRCC interfaces [18]. Consequently, the proposed formulation should not be regarded as a direct extension of steel–concrete composite models, but rather as an adaptation of their mechanical framework to a fundamentally different interface transfer mechanism and to the simultaneous time-dependent behaviour of both constituent materials.

Despite these differences, the overall structure of the mechanical problem remains unchanged. Once the axial force distribution $N(x,t)$ is computed for short-term and long-term conditions, the time evolution of interfacial slip (Eq. (5)), strains (Eq. 3), and stresses (Eq. 4) can be evaluated along the beam. The long-term analysis considers a time window ranging from t_0 = 28 to t_∞ = 70 years after strengthening. The experimental results and corresponding numerical predictions are presented and discussed in the following section.

3. Results

3.1. Experimental long-term response of composite beams

The long-term three-point loading bending tests (LT-3PBFT) were conducted on composite NSC–HPFRCC beams subjected to sustained service-level loading under controlled environmental conditions.

As presented in Section 2.2, the load value is fixed by computing the interfacial shear stress q (mode II) along the interface of composite member, see Fig. 8b, which is derived once the model calculates the variation of the internal actions (Fig. 8a), the strain (Fig. 8c, Fig. 8d) and stress fields (Fig. 8e, Fig. 8f) along the cross section at time t_0. This value is compared with the shear stress peak in mode II measured experimentally, see Fig. 5. Fig. 8 highlights the gap between the magnitude of both strain and stress fields arising in the existing NSC member and in the HPFRCC strengthening layer. The evolution of interfacial slip measured along the beam length over time is reported in Fig. 9e, Fig. 10 and Fig. 11. Results show a progressive increase of slip during the monitoring period.

Most of the slip development occurred during the initial phase of loading, followed by a gradual reduction in the slip rate over time. After several months, the slip evolution tended towards a stabilized trend, although a residual increase could still be observed throughout the six-month monitoring period. No visible signs of cracking or debonding were detected during the test, confirming that the applied load remained within the investigated service-level regime.

Although the long-term analysis predicts an increase of approximately 2000% in the tensile stress of the NSC substrate, this percentage reflects the very low initial stress level. The absolute tensile stress remains below the mean tensile strength of the NSC material throughout the 70-year service life, indicating that no cracking is expected under the considered service–level conditions. The spatial distribution of the interfacial shear stress along the beam length at selected time instants t = t_0 = 28 days is illustrated in Fig. 8b. The profile remained smooth and symmetric with respect to the beam mid-span, indicating a stable bond response and consistent load transfer between the NSC substrate and the HPFRCC overlay. The magnitude of axial force redistribution is consistent with the coupled evolution of interfacial deformation and internal force transfer. However, this relationship is governed by the interface stiffness: relative slip and transferred forces cannot be interpreted independently, since different levels of interface compliance modify the partition between relative displacement and internal force redistribution. This aspect is further investigated through the sensitivity analysis presented in Section 3.5.

3.2. Time-dependent redistribution of internal forces

The numerical model was further used to investigate the time evolution of internal axial forces and stresses within the composite beam. Fig. 9 presents the computed evolution of the axial force transferred across the interface at a selected section along the beam x = 0.5 L.

Results indicate a progressive redistribution of internal forces between the NSC substrate and the HPFRCC overlay over time. Immediately after load application, the load-sharing between the two layers reflects their elastic stiffness. As time progresses, differential creep and shrinkage induce a gradual transfer of axial force from the HPFRCC layer to the NSC substrate. This phenomenon is particularly pronounced during the early years following strengthening and tends to stabilize at later stages. The magnitude of axial force redistribution is consistent with the observed slip evolution, confirming the strong coupling between interfacial deformation and internal force transfer in composite cement-based systems.

3.3. Comparison between experimental measurements and numerical predictions

Fig. 10 and particularly Fig. 11 allow the comparison between the experimentally measured interfacial slip with the numerical predictions obtained from the proposed time-dependent cohesive model. The slips recorded by the 11 gauges are shown in those figures. Due to technical issues encountered during the experimental campaign, the gauge placed at x/L = 0.905 was lost.

A good agreement between experimental and numerical results is observed throughout the monitoring period. In particular, Fig. 11 displays together the experimental data and theoretical predictions. For clarity of the figure, only the slips detected by the 6 gauges on side A of the beam, as shown in Fig. 6b, have been plotted. The model reproduces the overall magnitude and temporal trend of the interfacial slip, particularly during the initial phase following load application, where time-dependent effects are most pronounced. It should be emphasised that the measured interface slips remain extremely small throughout the monitoring period, remaining within an absolute range of approximately ±0.002 mm over 160 days. At this scale, the observed differences between the numerical predictions and the experimental measurements should not be attributed exclusively to measurement uncertainty. They

UNCORRECTED PROOF

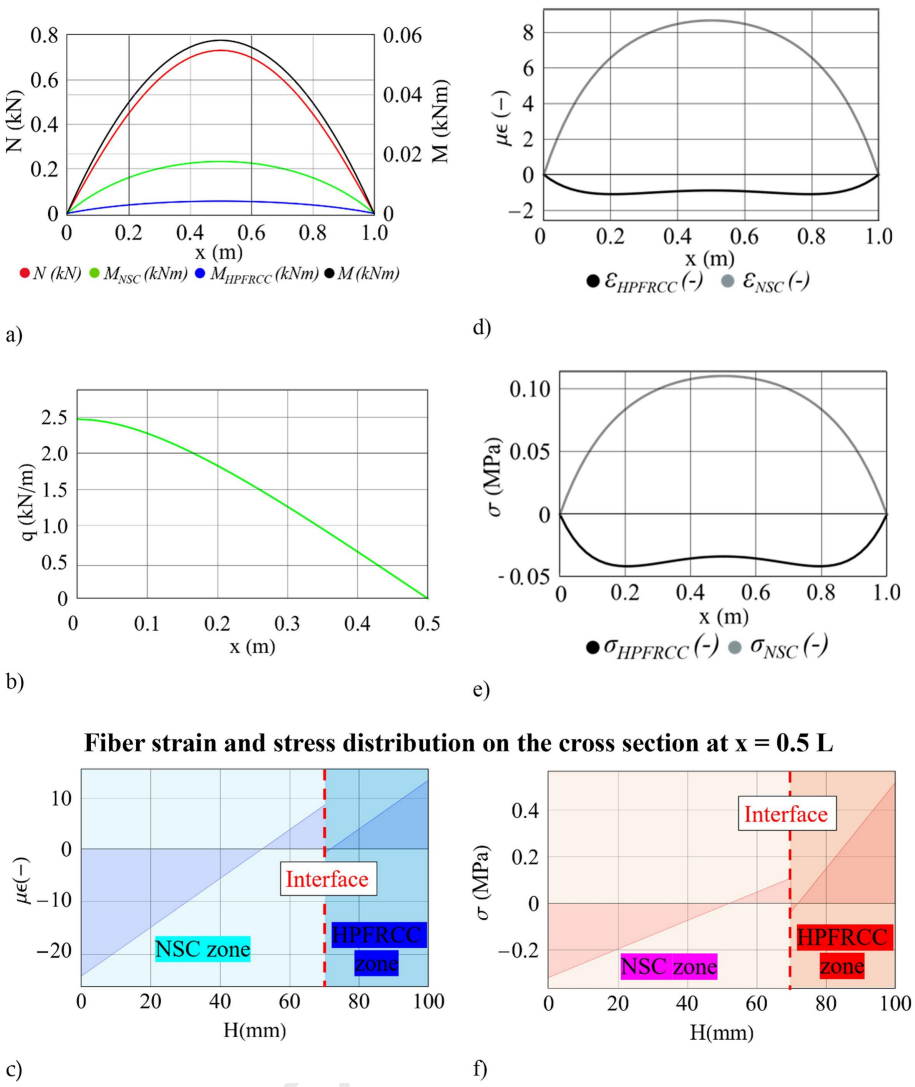

Fig. 8. Output provided by the elastic analysis (t = t_0 = 28 days after the pouring of the HPFRCC) of the composite NSC-HPFRCC beam: a) internal actions along the beam, b) shear stress along the interface, c), f) fiber strain and stress distribution on the cross-section at x = 0.5 L, d), e) fiber strain and stress along the interface.

are more realistically interpreted as the combined effect of the finite resolution of the measuring system, local micro-mechanical accommodation phenomena at the NSC–HPFRCC interface, and the simplified constitutive representation adopted for creep and shrinkage. The sensitivity analysis presented in this study further indicates that these small discrepancies do not modify the predicted mechanical response regime nor the resulting long-term stress redistribution. Overall, the comparison demonstrates that the proposed model is capable of reproducing the dominant mechanisms governing long-term interfacial behaviour in NSC–HPFRCC composite members under service loads.

3.4. Long-term stress evolution at the interface

The numerical model was used to evaluate the time-dependent evolution of normal stresses at the interface fibers of the NSC substrate and the HPFRCC overlay under sustained service loading. Fig. 9 presents the evolution of interface stresses along the beam mid-span for time instants ranging from the time of load application to the end of the simulated service life.

Immediately after load application, the stress distribution reflects the elastic regime between the two layers. As time progresses, a gradual redistribution of stresses is observed, driven by differential creep and shrinkage between the NSC substrate and the HPFRCC overlay. In particular, tensile stresses in the existing concrete substrate increase over time, while stresses in the strengthening layer progressively decrease. The most significant changes occur during the initial years after strengthening, followed by a slower rate of evolution at later stages.

The prediction of the spatial distribution of strains along the beam over 70 years is shown in Fig. 9 and Fig. 12. Strain profiles remain smooth and symmetric with respect to mid-span, with maximum slip developing near supports. The evolution of stress profile over time confirms the progressive nature of stress migration along the interface and its strong correlation with the observed interfacial slip development. Throughout the investigated time window, no stress levels exceeding the material strength were reached for the applied service load. Nevertheless, the results clearly demonstrate that time-dependent effects can significantly modify the stress state at the interface over the service life of strengthened members, even when the initial response remains within the elastic range.

It is also noted that the applied load level was intentionally kept very low to produce an almost linear behaviour of the shear stress-slip law. As a consequence, the measured slips (≈0.002 mm) and strains (≈20 με) lie close to the resolution limits of the displacement and strain sensors.

This limitation requires caution when interpreting the absolute numerical values and prevents the construction of a conventional statistical confidence interval, particularly because only one continuously mon-

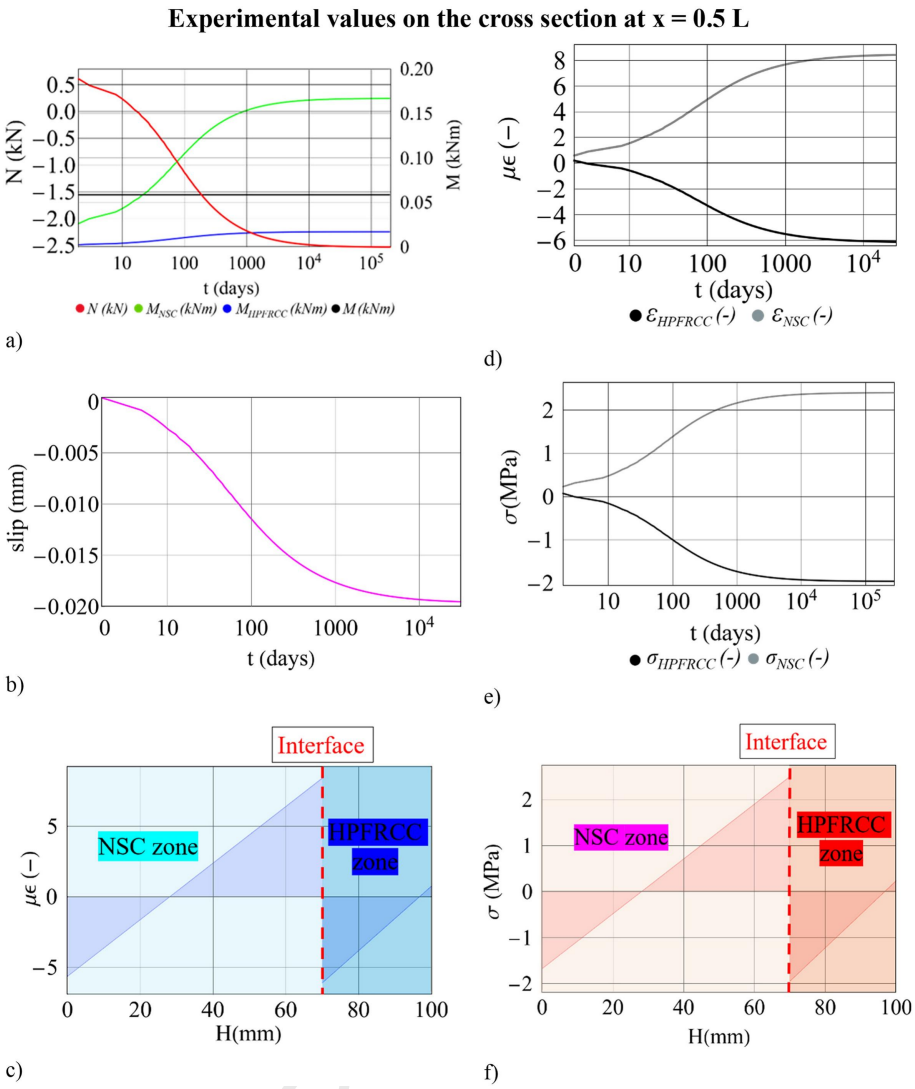

Fig. 9. Model output of long-term analysis (from t = 28 days until t = 70 years after the retrofitting) of the composite NSC-HPFRCC beam: a) internal actions, b) slip along the time, c), f) fiber strain and stress along the cross-section for t = 70 years, d), e) fiber strain and stress for t = 70 years.

itored long-term specimen was considered. Numerical predictions are complemented by a sensitivity envelope accounting for plausible variations in the interface stiffness and the principal time-dependent material parameters.

Such an analysis indicates that the low slip values are not attributable solely to the initial low load level. Rather, the measurements are consistent with a highly stiff, quasi-monolithic NSC–HPFRCC connection. Accordingly, the comparison between model and experiment should not be interpreted as a precise validation of sub-micron slip amplitudes, but as evidence that the proposed framework correctly identifies the governing response regime and the associated long-term stress redistribution.

3.5. Interpretation of the interface response and sensitivity to stiffness

The experimental observations indicate that the long-term response of the strengthened member may be interpreted through two limiting interface regimes.

In the first regime, corresponding to a carefully prepared interface exhibiting high bond stiffness, the relative displacement between the NSC substrate and the HPFRCC overlay remains negligible and the composite member behaves almost as a monolithic section. Under these conditions, the differential creep and shrinkage of the two cement-based materials cannot be accommodated through relative sliding. Instead, the incompatibility of the time-dependent deformations is mainly transferred into stress redistribution within the substrate, the strengthening layer and the interface. Such behaviour is consistent with the use of hydrodemolition, appropriate substrate moisture conditioning prior to casting and careful placement of the HPFRCC overlay, which are recognized as key requirements for obtaining highly efficient stress transfer in cementitious strengthening systems [36]. Conversely, a more compliant interface allows part of the differential deformation to be accommodated through interfacial slip. While this mechanism reduces the magnitude of the constraint-induced stresses, it simultaneously increases the relative displacement between the two layers and may progressively move the stress state towards the nonlinear branch of the cohesive law. Consequently, lower interface stresses should not necessarily be interpreted as an improvement in structural performance, since they may simply reflect the onset of progressive sliding and damage development.

To evaluate the transition between these limiting behaviours, a sensitivity analysis was performed, see Fig. 13. The interfacial shear stiffness K_{II} was varied around the experimentally calibrated value in order to simulate interfaces ranging from quasi-perfect bond to more compliant conditions representative of less effective substrate preparation or construction practice.

The resulting interface slip, internal axial forces and stress distributions were evaluated and compared with the reference solution

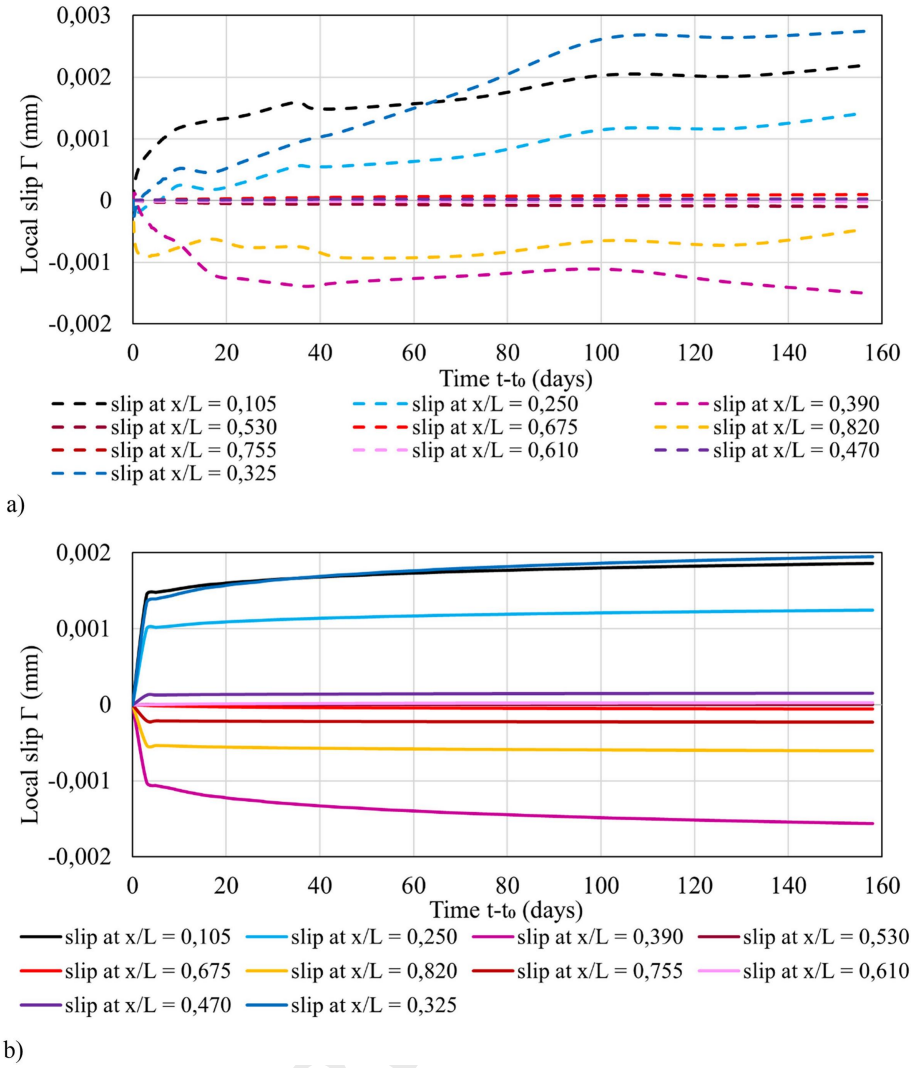

Fig. 10. a) Experimental slip-time evolution along the interface of composite NSC-HPFRCC beam. Plot of measurements for each strain gauge, b) Computation slip-time evolution along the interface of composite NSC-HPFRCC beam.

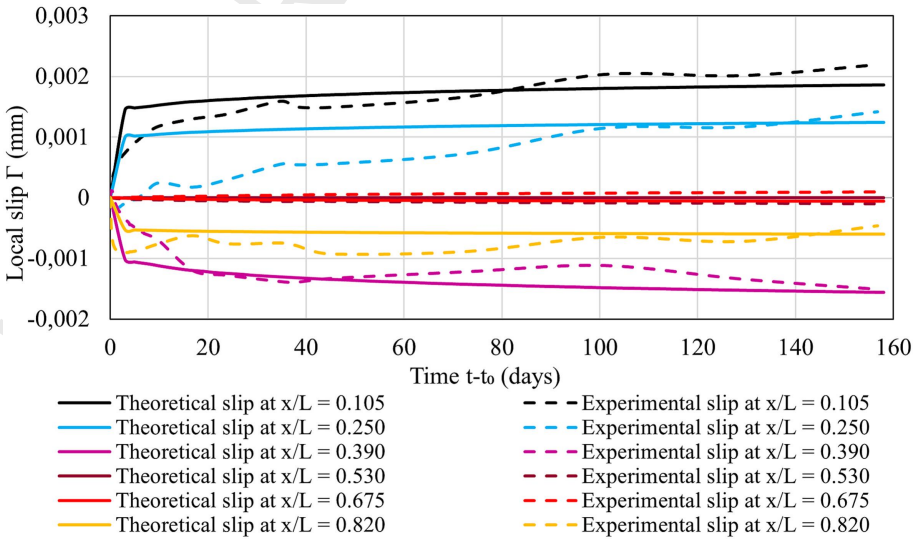

Fig. 11. Comparison of Experimental and Numerical Slip Values Along the Beam.

(Fig. 13). The objective of the sensitivity analysis is to assess how variations in interface stiffness modify the balance between relative displacement and internal force transfer and, consequently, the long-term stress redistribution within the strengthened member.

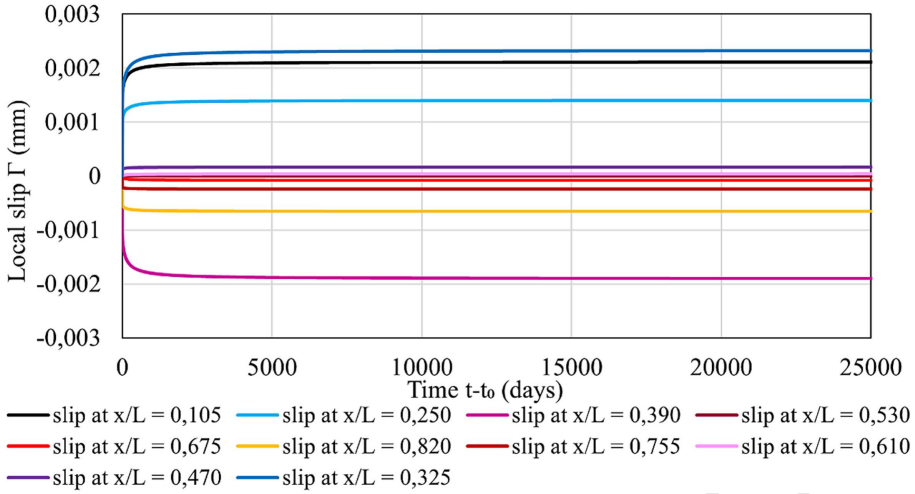

Fig. 12. Computation strain-time evolution for 70 years along the interface of the composite NSC-HPFRCC beam.

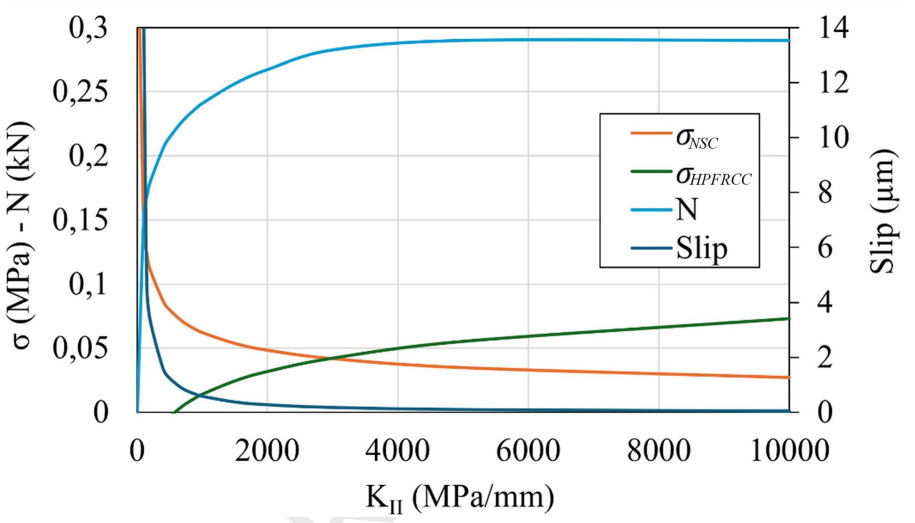

Fig. 13. Influence of the interfacial shear stiffness K_{II} on slip, external force N, and stress distribution between the NSC substrate (σ_{NSC} bottom fiber) and the HPFRCC strengthening layer (σ_{HPFRCC} top fiber) at x = 0.5 L.

The sensitivity analysis shows that interface stiffness governs the balance between relative slip and internal force transfer. As the interface stiffness decreases, larger relative displacements are accommodated at the interface, while the axial force redistribution between the NSC and HPFRCC layers is modified. Conversely, increasing the interface stiffness progressively constrains relative sliding and drives the composite system towards a higher degree of compatibility between the two layers.

These results confirm that interface slip cannot be interpreted independently from the corresponding stress state. A highly stiff interface may exhibit only micrometric relative displacements while still mobilising significant stresses, whereas a more compliant interface may accommodate larger slip with a different redistribution of internal forces and stresses. The mechanically relevant response therefore depends on the combined relationship between interface stiffness, strength and deformation capacity rather than on slip magnitude alone.

4. Conclusions

This study investigated the long-term interfacial behaviour of reinforced concrete members strengthened with high-performance fiber-reinforced cementitious composite (HPFRCC) overlays under sustained service loading. A time-dependent mechanical model combining linear viscoelasticity for the bonded materials with an experimentally calibrated cohesive law for the interface was proposed and assessed against a dedicated experimental campaign. Based on the results obtained, the following conclusions can be drawn:

Time-dependent interfacial effects are significant under service conditions. Even when the global response of the strengthened member remains within the elastic range, differential creep and shrinkage between the existing concrete substrate and the HPFRCC overlay induce progressive interfacial slip and stress redistribution over time. These effects are most pronounced during the early stages after strengthening but persist throughout service life.

Experimental observations support the capability of the proposed model. The model reproduces the main features of the long-term interface response. The measured relative displacements remained within the micrometric range. This observation is consistent with the high stiffness of the investigated NSC–HPFRCC interface and the resulting high degree of compatibility between the two cementitious layers.

Stress redistribution at the interface cannot be neglected. Numerical results highlight a progressive migration of stress between the strengthening layer and the existing concrete substrate, leading to a substantial increase in tensile stresses in the substrate over time. Although the relative increase exceeds 2000% because of the very

low initial stress level, the absolute tensile stress remains below the mean tensile strength of the NSC throughout the investigated service life.

Interface stiffness governs the balance between compatibility, slip and stress redistribution. A highly stiff interface strongly constrains relative sliding and promotes composite action between the NSC substrate and the HPFRCC overlay, but may mobilize significant interfacial stresses over only micrometric relative displacements. Conversely, a more compliant interface allows larger relative displacements and modifies the transfer and redistribution of internal forces between the two layers. Consequently, the magnitude of interface slip alone cannot be used as an indicator of proximity to damage or interface performance. The response must instead be assessed by considering interface stiffness together with strength and deformation capacity. The present formulation describes this time-dependent pre-damage response and provides a basis for its subsequent implementation in more general numerical frameworks, including finite-element analyses.

Serviceability-based modelling provides a rational assessment framework. The adoption of an experimentally justified linear-elastic bond regime, combined with service-load calibration, enables a consistent application of viscoelastic theory to cement-based composite systems. This approach avoids extending the linear formulation beyond its experimentally justified range and provides a physically sound basis for long-term performance evaluation. It is worth noting that the substantial stress redistributions shown in Fig. 9e do not imply nonlinear creep behaviour. Stress levels remain below approximately 2 MPa throughout the 70-year service life, which is well within the range where the linear creep formulation of the CEB-FIP Model Code is applicable [37].

Implications for design and assessment of strengthened structures. The proposed formulation provides a mechanical framework for evaluating the long-term pre-damage response of HPFRCC-strengthened concrete members by explicitly accounting for time-dependent interfacial behaviour. It can support the assessment of interface compatibility and stress redistribution under service conditions and provide a basis for identifying potentially critical interface conditions in strengthened members.

5. Limitations and outlook

The experimental program was intentionally designed as a mechanical analysis of the long-term NSC–HPFRCC interface response using a simplified small-scale configuration suitable for continuous monitoring over several months. Such a static scheme provides evidence of the interface behaviour under different sectional stress distributions and global deformation levels; nevertheless, additional tests on larger structural members and a broader range of interface properties would be valuable to further extend the validation domain of the proposed formulation and assess possible structural-size effects. Further developments will focus on extending the present time-dependent framework to more general loading and environmental conditions, including differential thermal actions and cyclic loading. Particular attention will be devoted to coupling the pre-damage formulation developed here with the nonlinear mixed-mode cohesive approach previously developed by the Authors [18,34], allowing the evolution of the bonded system towards damage initiation and subsequent delamination propagation to be investigated. Such developments can be implemented within finite-element frameworks for the analysis of more complex structural configurations and for assessing the combined influence of interface stiffness, strength and deformation capacity on the long-term performance of strengthened members.

The rationale for investigating the pre-damage regime is precisely to establish this link between the relative stiffness of the substrate, overlay and interface, the magnitude of interfacial slip, and the time-dependent response of the constituent materials. In a broader framework, this would allow the combined effects of sustained service loading, creep and environmental actions to be assessed in terms of their potential to progressively drive local regions of the interface towards damage initiation. Coupling this information with a nonlinear damage-propagation model would ultimately provide engineers with a means of identifying critical regions where premature interface degradation could compromise composite action and consequently affect the load-bearing capacity of the strengthened member.

CRediT authorship contribution statement

J.A.L. Sanchez: Writing – original draft, Validation, Software, Conceptualization, Investigation, Methodology. **V. Savino:** Writing – original draft, Software, Methodology, Conceptualization. **L. Lanzoni:** Writing – review & editing, Investigation, Supervision, Formal analysis, Methodology. **A.M. Tarantino:** Visualization, Supervision, Conceptualization, Methodology. **M. Viviani:** Writing – review & editing, Visualization, Supervision, Resources, Conceptualization.

Declaration of competing interest

The authors declare that they have no known competing financial interests or personal relationships that could have appeared to influence the work reported in this paper.

Acknowledgements

The Authors gratefully acknowledge the financial support provided by the Haute École d'Ingénierie et de Gestion du Canton de Vaud (HEIG-VD), HES-SO University of Applied Sciences and Arts Western Switzerland, and by Innosuisse through the FieldEarth project. The financial support provided by the Italian Ministry of University and Research (MUR) within the framework of the FISA-2022 project *"Earth-Tech"* (code 00183; CUP: E93C24000250001) is gratefully acknowledged. LL gratefully acknowledges the financial support of the MUR through the research grant project PRIN 2026 "LACES – Low-impact Advanced Concrete Engineering Systems: Mechanical and Multiphysics Modelling, Experimental Validation and Design Guidelines" (prot. 2026PRP438).

Data availability

Data will be made available on request.

References

[1] Delatte NJ, Wade DM, Fowler DW. Laboratory and field testing of concrete bond development for expedited bonded concrete overlays. ACI Mater J 2000;97.
[2] Krstulovic-Opara N, Toutanji H. Infrastructural repair and retrofit with HPFRCCs. High Perform Fiber Reinf Concr Compos 1995;2:423–42.
[3] Yang J, Xia J, Zhang Z, Zou Y, Wang Z, Zhou J. Experimental and numerical investigations on the mechanical behavior of reinforced concrete arches strengthened with UHPC subjected to asymmetric load. Structures 2022;39:1158–75. https://doi.org/10.1016/j.istruc.2022.03.087.
[4] Al-Osta MA, Isa MN, Baluch MH, Rahman MK. Flexural behavior of reinforced concrete beams strengthened with ultra-high performance fiber reinforced concrete. Constr Build Mater 2017;134:279–96. https://doi.org/10.1016/j.conbuildmat.2016.12.094.
[5] Denarié E. Rehabilitation of concrete structures using Ultra-High Per- formance Fiber Reinforced Concrete n.d.
[6] Experimental Investigation on Reinforced Ultra-High-Performance Fiber-Reinforced Concrete Composite Beams Subjected to Combined Bending and Shear. ACI Struct J 2013;110. https://doi.org/10.14359/51684405
[7] Yin H, Teo W, Shirai K. Experimental investigation on the behaviour of reinforced concrete slabs strengthened with ultra-high performance concrete. Constr Build Mater 2017;155:463–74. https://doi.org/10.1016/j.conbuildmat.2017.08.077.
[8] Franciosi M, Kasser M, Viviani M. Digital twins in bridge engineering for streamlined maintenance and enhanced sustainability. Autom Constr 2024;168:105834. https://doi.org/10.1016/j.autcon.2024.105834.
[9] Barbieri L, Lanzoni L, Marchetti R, Iotti S, Tarantino AM, Lancellotti I. Shot-earth as sustainable construction material: chemical aspects and physical performance. Sustainability 2024;16:2444. https://doi.org/10.3390/su16062444.

UNCORRECTED PROOF

[10] Franciosi M, Savino V, Lanzoni L, Tarantino AM, Viviani M. Long-term creep behavior of new earth composite materials. J Mater Civ Eng 2025;37:04025131. https://doi.org/10.1061/JMCEE7.MTENG-17216.
[11] Iotti S, Lanzoni L, Tarantino AM, Viviani M. Rethinking excavated-earth concrete: water transport in sustainable earthcretes. J Build Eng 2026;120:115409. https://doi.org/10.1016/j.jobe.2026.115409.
[12] Yang Y, Liu Z, Tang H, Peng J. Deflection-based failure probability analysis of low shrinkage-creep concrete structures in presence of non-stationary evolution of shrinkage and creep uncertainties. Constr Build Mater 2023;376:131077. https://doi.org/10.1016/j.conbuildmat.2023.131077.
[13] Granju J-L, Sabathier V, Turatsinze A, Toumi A. Interface between an old concrete and a bonded overlay: debonding mechanism. Interface Sci 2004;12:381–8. https://doi.org/10.1023/B:INTS.0000042336.03156.cb.
[14] Safdar M, Matsumoto T, Kakuma K. Flexural behavior of reinforced concrete beams repaired with ultra-high performance fiber reinforced concrete (UHPFRC). Compos Struct 2016;157:448–60. https://doi.org/10.1016/j.compstruct.2016.09.010.
[15] Lampropoulos AP, Paschalis SA, Tsioulou OT, Dritsos SE. Strengthening of reinforced concrete beams using ultra high performance fiber reinforced concrete (UHPFRC). Eng Struct 2016;106:370–84. https://doi.org/10.1016/j.engstruct.2015.10.042.
[16] Farzad M, Shafieifar M, Azizinamini A. Experimental and numerical study on bond strength between conventional concrete and Ultra High-Performance Concrete (UHPC). Eng Struct 2019;186:297–305. https://doi.org/10.1016/j.engstruct.2019.02.030.
[17] Yin H, Shirai K, Teo W. Numerical model for predicting the structural response of composite UHPC–concrete members considering the bond strength at the interface. Compos Struct 2019;215:185–97. https://doi.org/10.1016/j.compstruct.2019.02.040.
[18] Savino V, Lanzoni L, Tarantino AM, Viviani M. A cohesive model to predict the loading bond capacity of concrete structures repaired/reinforced with HPFRC/UHPFRC and stressed to mixed mode. Cem Concr Compos 2020;112:103673. https://doi.org/10.1016/j.cemconcomp.2020.103673.
[19] Diab H, Wu Z. Nonlinear constitutive model for time-dependent behavior of FRP-concrete interface. Compos Sci Technol 2007;67:2323–33. https://doi.org/10.1016/j.compscitech.2007.01.018.
[20] Habel K, Denarie E. Time dependent behavior of elements combining ultra-high performance fiber reinforced concretes (UHPFRC) and reinforced concrete n.d.
[21] Cohesive Crack with Rate-Dependent Opening and Viscoelasticity: I. Mathematical Model and Scaling n.d.
[22] Granju J-L. Debonding of thin cement-based overlays. J Mater Civ Eng 2001;13:114–20. https://doi.org/10.1061/(ASCE)0899-1561(2001)13:2(114).
[23] Marcello Tarantino A, Dezi L. Creep effects in composite beams with flexible shear connectors. J Struct Eng 1992;118:2063–80. https://doi.org/10.1061/(ASCE)0733-9445(1992)118:8(2063).
[24] EN 1992-1-1. Eurocode 2: Design of concrete structures – Part 1-1: General rules and rules for buildings 2004.
[25] Bentz DP, De La Varga I, Muñoz JF, Spragg RP, Graybeal BA, Hussey DS, et al. Influence of substrate moisture state and roughness on interface microstructure and bond strength: Slant shear vs. pull-off testing. Cem Concr Compos 2018;87:63–72. https://doi.org/10.1016/j.cemconcomp.2017.12.005.
[26] Gulyas RJ, Wirthlin GJ, Champa JT. Evaluation of Keyway Grout Test Methods for Precast Concrete Bridges. PCI J 1995;40:44–57. https://doi.org/10.15554/pcij.01011995.44.57.
[27] CEN EN 14651. Test method for metallic fibered concrete - Measuring the flexural tensile strength (limit of proportionality (LOP), residual) 2005.
[28] Savino V, Lanzoni L, Tarantino AM, Viviani M. Tensile constitutive behavior of high and ultra-high performance fiber-reinforced-concretes. Constr Build Mater 2018;186:525–36. https://doi.org/10.1016/j.conbuildmat.2018.07.099.
[29] CEB-FIP Model Code 1990. C.E.B. Bulletin d'Information n.190 1988.
[30] CEN EN 12390-3. Compressive strength of test specimens 2003.
[31] CEN EN 13412. Products and systems for the protection and repair of concrete structures - Determination of modulus of elasticity in compression 2006.
[32] CNR-DT 204. Guidelines for design, construction and production control of fiber reinforced concrete structures 2006.
[33] Savino V, Lanzoni L, Tarantino AM, Viviani M. An extended model to predict the compressive, tensile and flexural strengths of HPFRCs and UHPFRCs: Definition and experimental validation. Compos B Eng 2019;163:681–9. https://doi.org/10.1016/j.compositesb.2018.12.113.
[34] Savino V, Lanzoni L, Tarantino AM, Viviani M. A cohesive FE model for simulating the cracking/debonding pattern of composite NSC-HPFRC/UHPFRC members. Constr Build Mater 2020;258:119516. https://doi.org/10.1016/j.conbuildmat.2020.119516.
[35] ASTM C512M-15. Standard test method for creep of concrete in compression 2015.
[36] Habel K, Viviani M, Denarié E, Brühwiler E. Development of the mechanical properties of an Ultra-High Performance Fiber Reinforced Concrete (UHPFRC). Cem Concr Res 2006;36:1362–70. https://doi.org/10.1016/j.cemconres.2006.03.009.
[37] CEB_FIP_model_code_1990_ing n.d.

UNCORRECTED PROOF